ELSEVIER

Materials and Design 21 (2000) 287–295

Materials & Design

Superplastic roll forming of Ti alloys

B.P. Bewlay[a,*], M.F.X. Gigliotti[a], F.Z. Utyashev[b], O.A. Kaibyshev[b]

[a] *General Electric Corporate Research and Development, P.O. Box 8, Schenectady, NY 12301, USA*
[b] *Institute for Metals Superplasticity Problems, Russian Academy of Sciences, Ufa, 450001 Bashkortostan, Russia*

Abstract

The high cost of aerospace alloys and their components makes them prime candidates for net-shape manufacturing techniques. Conventional processes for manufacturing disk components include hammer, hot die, and isothermal forging. This paper will examine the potential of a revolutionary approach for the manufacture of aircraft engine disks, superplastic roll forming. The process of superplastic roll forming, developed at the Institute for Metals Superplasticity Problems, Ufa, employs pairs of small opposed rollers to shape a cylindrical workpiece into a complex axisymmetric shape by simultaneously adjusting the roll gap and by moving the rolls radially outward on the workpiece while it is rotated about its axis of symmetry. Both the workpiece and the rolls are maintained at temperatures close to the beta transus. This paper will describe metallurgical evaluations of superplastically roll formed disks of alloy VT25. The evaluations of the disks included microstructure, crystallographic texture, heat treatment response, tensile strength, stress rupture resistance, and ultrasonic characteristics. The disk microstructures were found to be uniform and without any strongly textured colonies. Mechanical properties of the roll formed VT 25 were compared with those of Ti-6242S, IMI834, and conventionally forged VT25. The RF VT25 disk was found to possess low ultrasonic noise and high inspectability, which provided an increase in signal to noise for synthetic flaws.

Keywords: Superplastic roll forming; VT25 alloy; Aircraft engine disks

1. Introduction

The present paper will describe an evaluation of the application of roll forming to the manufacture of turbine engine disks. Roll forming is a revolutionary method that has been developed for the manufacture of disks. Roll forming possesses improved potential net shape manufacturing capability over conventional forging approaches because it can provide greater utilization of the input material. In the manufacture of forgings for aerospace applications, the cost of the input billet material is one of the primary components of the cost of premium grade forgings. Thus, net shape manufacturing processes play a key role in the aerospace business.

In the aerospace industry, the selection of the optimum forming technique depends on the size of the part to be made, the capacity of the equipment, the complexity of the required shape, and the component cost. In addition, the correct deformation process parameters (strain, strain rate, and temperature) are required in order to generate the combination of mechanical properties, such as tensile strength, fatigue performance, and creep properties, that are required in the finished part. Thus, for roll forming to be successfully applied to the manufacture of aerospace components, it must satisfy many requirements.

Roll forming technology has been practised in several different forms, such as metal spinning, axial roll forming, and shear forming [1]. One of the earliest applications of roll forming concepts was the Slick mill [2], in which a cylindrical pancake was clamped between two dies. One die was offset at an angle to the other and it was rotated, thereby rotating the workpiece and the opposing die. Fig. 1 shows a schematic diagram of

* Corresponding author.

0261-3069/00/$ - see front matter
PII: S0261-3069(99)00089-8

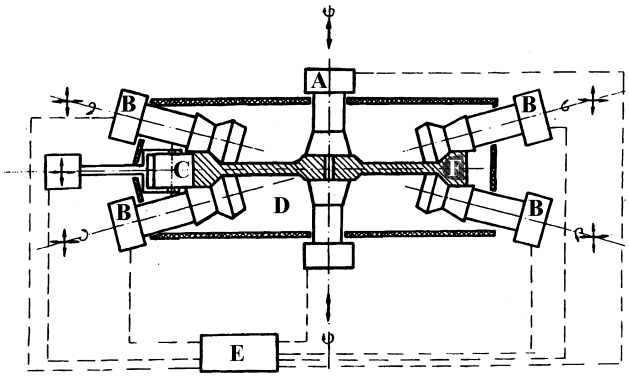

Fig. 1. Schematic diagram of the SRD800 roll forming mill, showing (A) the main drive shaft, (B) the axial–radial working rolls, (C) the outer radial working rolls, (D) the furnace cavity, (E) the controls, and (F) the workpiece.

roll forming of a disk using the SRD800 mill at the Institute for Metals Superplasticity Problems, Ufa, Russia. The innovative design of this mill adds several degrees of freedom of roll movement in comparison to prior roll forming schemes. The workpiece of the starting material is rotated about its axis of symmetry by the main shaft of the roll forming mill (A). There are small rollers (B) that can move in the radial direction (r) and the axial direction (z) with respect to the workpiece. These axial–radial working rolls (B) are brought into contact with the workpiece and pinch the workpiece in the radial direction. These rollers are then moved in both the axial and radial directions according to a pre-designed profile to form the component. The roll forming operation is performed in a closed furnace with the aid of computer control. A photograph of the initial stage of roll forming of a disk is shown in Fig. 2.

The present paper describes the metallurgical and ultrasonic characteristics of roll formed (RF) disks of alloy VT25 [3]. VT25 is a near alpha titanium alloy with a composition of Ti–6.4Al–2.2Sn–1.9Zr–2.0Mo–1.1W–0.2Si (compositions are given in weight percent). The disk microstructures, crystallographic texture, tensile strength, stress rupture performance, and ultrasonic characteristics (as measured using C-scans) will be described. These data are compared with similar data for conventionally processed VT25.

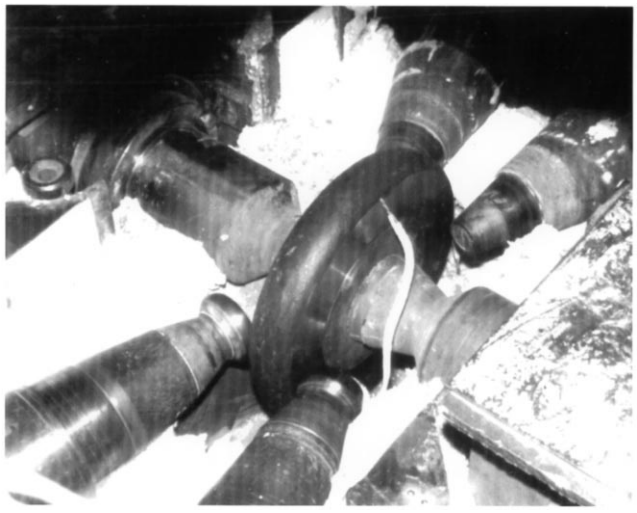

Fig. 2. Photograph of the initial stage of roll forming of a disk. The photograph shows the initial workpiece, the main drive shaft, the axial–radial working rolls, and the furnace.

2. Experimental

The two sample shapes that were roll formed for metallurgical evaluations are shown in Fig. 3. Fig. 3a shows a simple disk shape together with the general disposition of the forming rolls. The view is rotated from the actual orientation used in practice to illustrate the process. Fig. 3b shows a RF disk with more complex internal and external profiles. Fig. 3b shows the as-RF shape and the finished shape that was required for ultrasonic inspection. The internal diameter of the RF component in Fig. 3b is closer to the required shape than the conventionally forged component because the conventional forging operation is capable of only precisely forming the external profile. As a result, roll forming requires less billet material than the conventional forging process for this specific shape. The disk shape shown in Fig. 3a was produced in order to generate a RF component from which samples could be machined for mechanical property evaluations.

The RF disks were sliced and samples were subjected to the conventional VT25 heat treatment of a solution at 950°C for 1 h followed by aging at 530°C for 6 h. Further solutioning heat treatments were performed to adjust the volume fraction of primary αTi. The macrostructures and the microstructures of the disks were examined using light microscopy and scanning electron microscopy. Electron back-scatter pattern analyses (EBSP) measurements were also performed. Scans were performed of selected regions at the hub, web and rim of the disk. Diffraction patterns were obtained at each point and the orientation of each grid

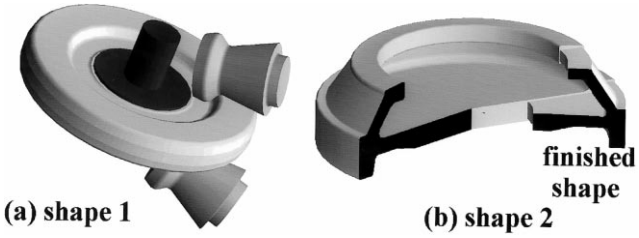

Fig. 3. Schematic diagram of the roll formed shapes that were evaluated: (a) a simple axially symmetric disk; and (b) a disk with flanges and more complex internal profile.

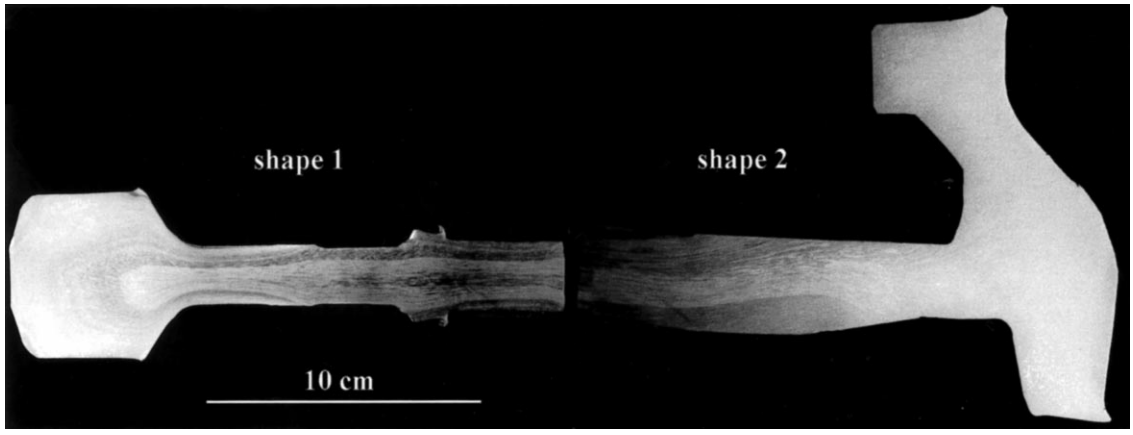

Fig. 4. Longitudinal sections of the RF VT25 disks.

point was determined by analysis of the diffraction pattern. The (0001) pole was determined from the diffraction data and a level of grey assigned to the grid position based on a spherical grey-scale map of the angle of the (0001) pole. Each level of grey represents a unique crystallographic orientation. Each scan was 560 μm^2 and employed a step size of 2 μm.

Samples were machined from disk shapes 1 and 2 for tensile and stress rupture measurements. Separate samples were machined such that the longitudinal axes of the tensile samples were parallel to both the axial and radial directions in the disk. A 50-mm-thick slice was also cut from the disk and tensile samples were machined such that the longitudinal axes of the tensile samples were parallel to the tangential direction in the disk. The samples that were subjected to the 950°C treatment were machined from shapes 1 and 2, and the samples that were subjected to the treatments at higher temperatures were machined from shape 1. Right rectangular prisms were machined from the RF disks in order to perform C-scans using ultrasonic immersion measurements at 20 MHz. The RF VT25 ultrasonic data were compared with those of samples from conventionally forged Ti-6242.

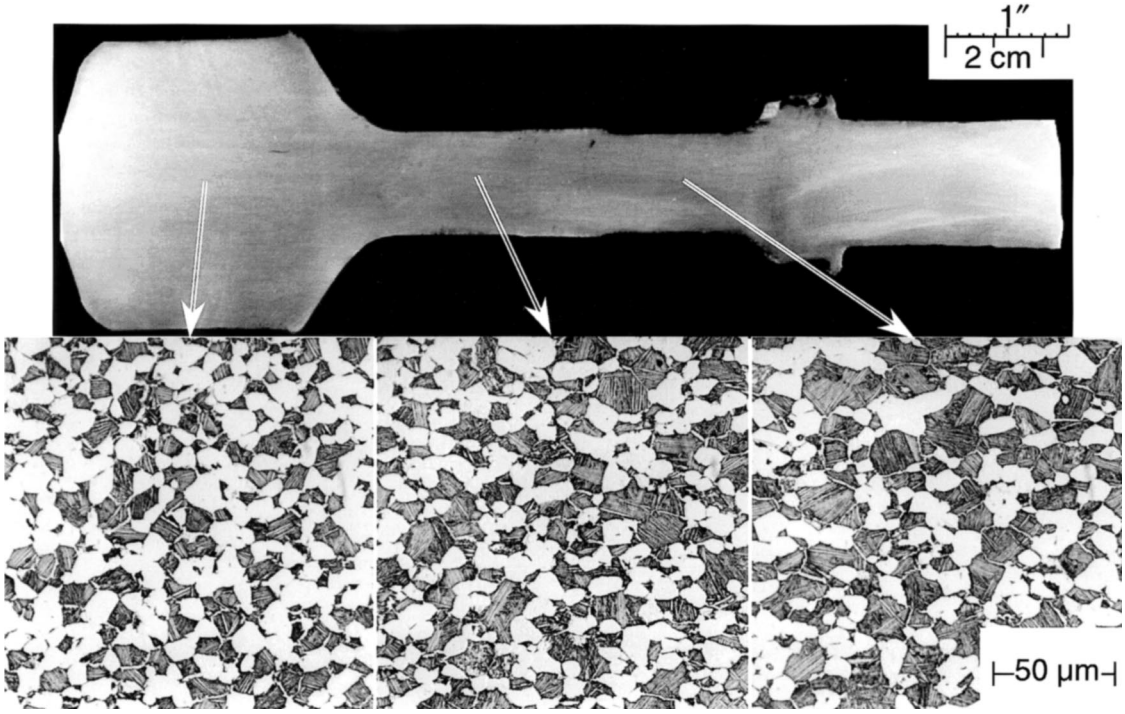

Fig. 5. Macrostructure and microstructures at the mid-plane of the longitudinal section of RF disk shape 1 after the 970°C + 530°C heat treatment. The radial direction is horizontal in these figures.

3. Results

The present section will describe the examinations of the RF VT25 disks and will include microstructural analyses, texture analyses, ultrasonic examination, and mechanical property determination. The tensile properties and stress rupture behavior will also be described.

4. RF disk microstructure and texture analyses

Longitudinal sections of the macrostructures of the RF VT25 disks after heat treatment are shown in Fig. 4a,b. The disks possessed a fine grain size throughout the whole section, although some macroscopic flow lines could be observed in the heat-treated slices. It is thought that these may have been due to segregation in

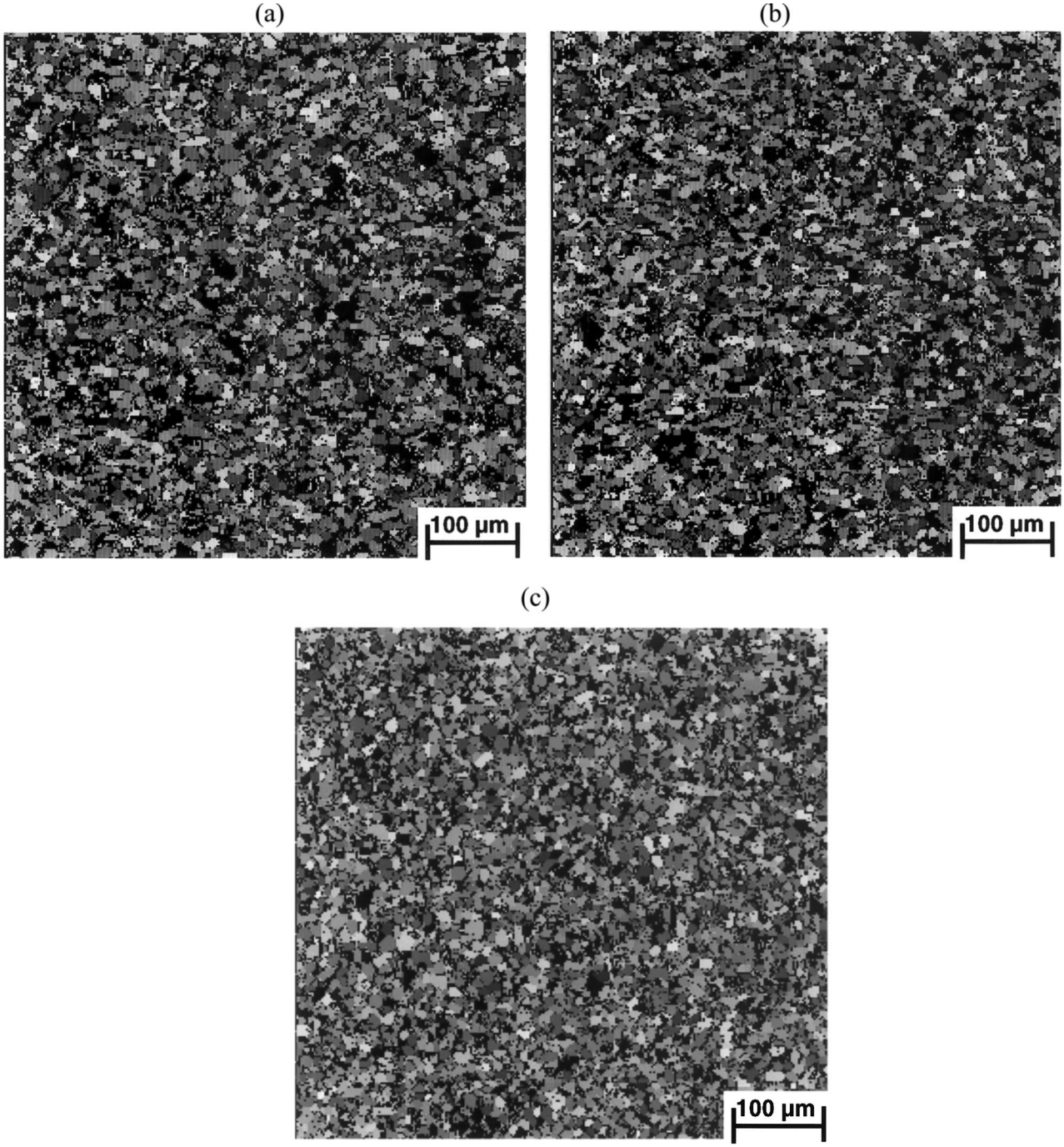

Fig. 6. EBSP patterns showing the primary α Ti grain orientation in the RF VT25 disk at (a) the hub, (b) the web, and (c) the rim.

the cast ingot. The disk shape shown in Fig. 4a was roll formed by pushing the rollers together at the hub of the workpiece and then withdrawing the rollers in the radial direction. In this manner, the simple shape was formed by a type of radial extrusion in which the diameter of the disk was increased to a diameter greater than twice that of the initial billet.

The microstructure of the hub, web, and rim of the disk shown in Fig. 4a were examined both at the mid-plane, and at a distance of 1 mm from the surface of the disk. A higher magnification micrograph of disk shape 1 after the conventional VT25 heat treatment is shown in Fig. 5 together with micrographs of the disk at three regions progressing from the hub to the outer rim. The microstructure possessed a uniform $\alpha + \beta$ Ti structure throughout the disk with an α Ti grain size of ~ 10 μm. There was also an α Ti case ~ 100 mm thick on the surface of the disk which was probably due to oxygen penetration into the Ti at the rolling temperature. This region was removed prior to mechanical property evaluation.

The orientation images obtained using EBSP of the hub, web, and rim of the RF VT25 disk are shown in Fig. 6. These images show the primary α Ti grain orientation as a function of grey-scale. These EBSP data indicated that the microstructure had a general tweed pattern and each of the primary α Ti grains in the hub, web and rim possessed different crystallographic orientations. Fig. 6 indicates that there was no texture in the α Ti in the hub section of the disk. The hub had experienced the least deformation. In the web and rim regions, which are regions of higher deformation, again no α Ti texture was observed. Of particular relevance to fatigue properties, these EBSP measurements indicate that there were no colonies present [4].

(0001) Pole figures are shown in Fig. 7a,b for both the web and the rim of the RF disk. Again, these pole figures suggest that there is essentially no texture in the web and the rim of the disk. Thus, the microstructure and microtexture data are consistent with the disk being superplastically formed, although the strain rates in the deformation volumes immediately beneath the rollers are higher than those generally reported for superplasticity of Ti alloys in both pure tension and compression ($\sim 10^{-3}$ s^{-1}) [5].

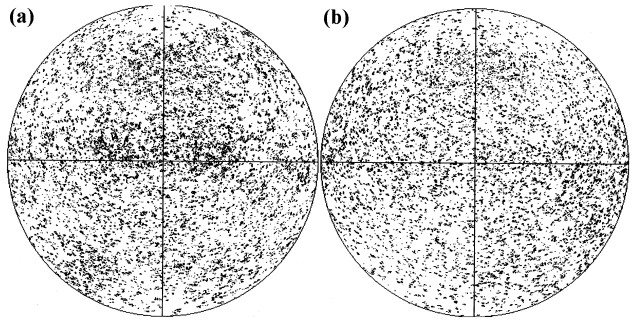

Fig. 7. (0001) Pole figures of grains within the RF VT25 disk: (a) the disk web; and (b) the rim of the disk.

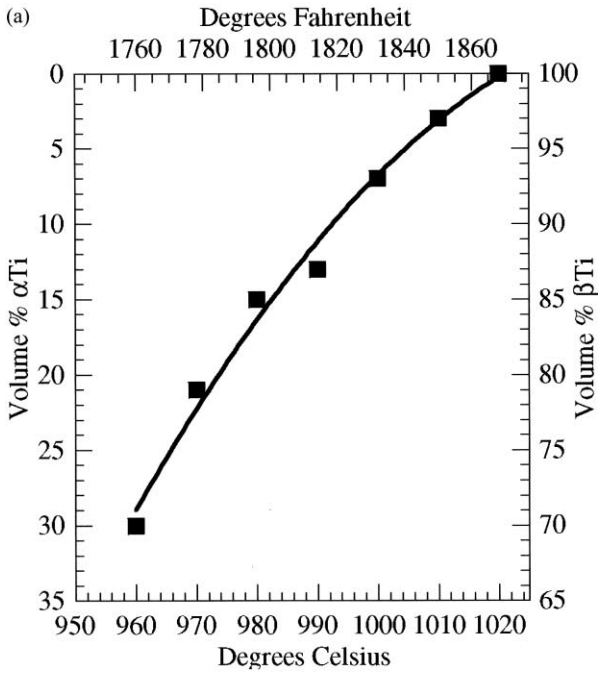

Fig. 8. Microstructure of the RF VT25 after alternate heat treatments to reduce the volume fraction primary α Ti. (a) The volume fraction α Ti as a function of solutioning temperature. (b) The microstructure after 1010°C + 530°C heat treatment.

The volume fraction of primary α Ti was measured

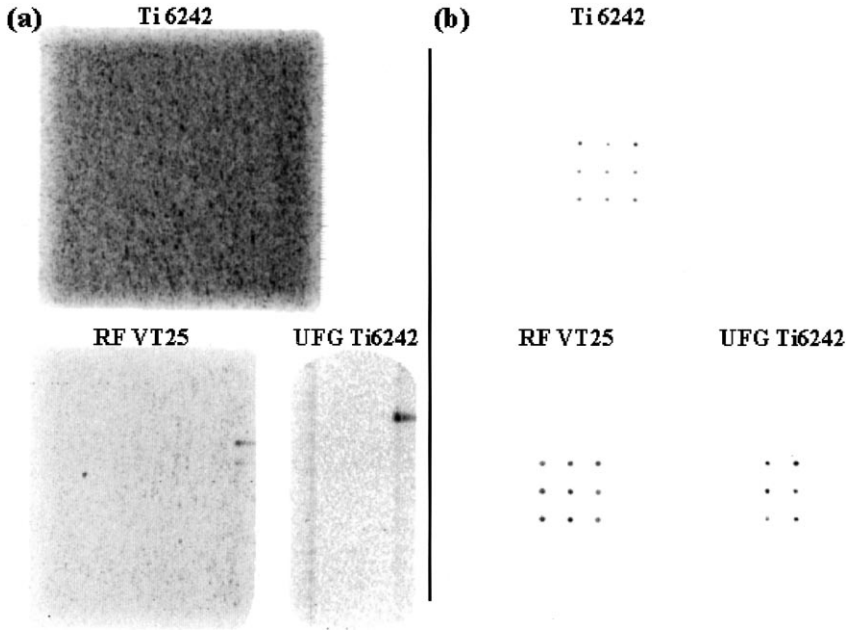

Fig. 9. C-scans at 20 MHz of 38-mm-thick blocks containing 0.8-mm-diameter flat bottom holes drilled from the bottom to a depth of 25 mm below the top surface. The blocks were machined from a conventional Ti-6242 forging, the RF VT25 disk, and a uniform fine grain (UFG) Ti-6242 forging. (a) The back-scattered noise. (b) The signal from holes.

metallographically using water quenched samples that were subjected to 1 h anneals at temperatures from 960°C to 1030°C. Fig. 8a shows the transus approach curve for the RF VT25, and it indicates a β transus of 1020°C. The RF VT25 microstructures were uniform throughout the entire specimens, and this uniformity permitted mechanical property evaluation of material with a low-volume fraction of primary α Ti and uniform small colonies of transformed β Ti. Fig. 8b shows the microstructure of the RF VT25 after the selected alternate solution heat treatment at 1010°C for 1 h followed by aging at 530°C for 6 h; the microstructure contained a volume fraction of primary α Ti of ~ 0.15 with the balance being transformed β Ti. The β Ti grain size was ~ 50 μm and there were many separate colonies within the β Ti grains.

5. Ultrasonic evaluations

Fig. 9 shows ultrasonic C-scans of the blocks that were machined from the conventional Ti-6242 forging, the RF VT25 disk, and also a uniform fine grain (UFG) processed Ti-6242 forging. The Ti-6242 block had dimensions of $50 \times 50 \times 38$ mm. Flat bottom holes were machined in order to provide synthetic flaws of a

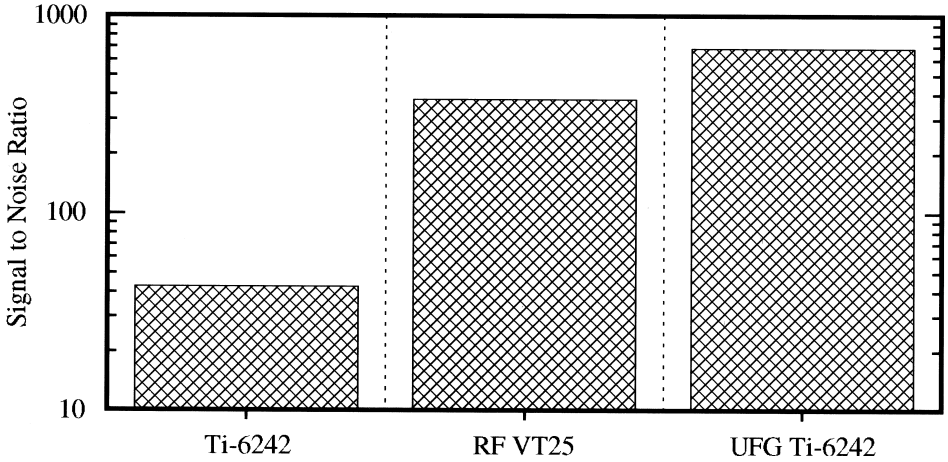

Fig. 10. Comparison of the ultrasonic signal to noise ratio from the 0.8 mm diameter flat bottom holes in the blocks machined from the Ti-6242, the RF VT25, and the UFG Ti-6242.

Table 1
Tensile behavior of RF VT25, including 0.2% yield stress, UTS, % elongation and reduction in area[a]

Temperature (°C)	Sample orientation	Heat treatment (°C)	Yield stress (MPa)	UTS (MPa)	Elongation (%)	Reduction in area (%)
20	Longitudinal	950	906	1052	20	43
400	Longitudinal	950	551	785	23	55
500	Longitudinal	950	492	731	24	63
550	Longitudinal	950	477	685	26	69
600	Longitudinal	950	397	587	31	78
23	Tangential	970	976	1089	16	46
260	Tangential	970	706	884	18	55
454	Tangential	970	621	801	18	60
538	Tangential	970	590	740	22	73
593	Tangential	970	559	668	23	82
649	Tangential	970	422	535	37	94
23	Tangential	1010	945	1103	12	31
260	Tangential	1010	786	910	14	43
454	Tangential	1010	609	821	15	53
538	Tangential	1010	586	769	18	67
593	Tangential	1010	545	683	22	78
649	Tangential	1010	436	564	35	86

[a] Data are shown from samples that were subjected to solution temperatures of 950°C, 970°C and 1010°C.

well-defined acoustic reflectance. For the Ti-6242 and the RF VT25, nine 0.8-mm-diameter flat bottom holes were machined in the blocks to a depth of 25 mm below the top surface. Only six holes were machined in the UFG Ti-6242. Fig. 9a shows the back-scattered noise and Fig. 9b shows the ultrasonic signal from the flat bottom holes. In Fig. 9a the gain was set to amplify the noise and the ultrasonic information was gated to exclude the signal from the flat bottom holes. In Fig. 9a, the bright regions are low noise and the dark regions are high noise. These images indicate that the forged Ti-6242 possesses a higher ultrasonic noise level than both the RF VT25 and the UFG Ti-6242.

The signals from the flat bottom holes are shown in Fig. 9b; the C-scan data was gated to a depth of ~25 mm below the top surface to select only the tips of the 0.8-mm flat bottom holes. The images show that the signal from the flat bottom holes is larger in the RF VT25 and UFG Ti-6242 than in the Ti-6242 forging. These data suggest that the attenuation of the signal from the synthetic defects is less in the RF VT25 and UFG Ti-6242. Fig. 10 shows the signal to noise ratio from the 0.8-mm flat bottom holes for Ti-6242, RF VT25 and UFG Ti-6242. The signal to noise ratios for

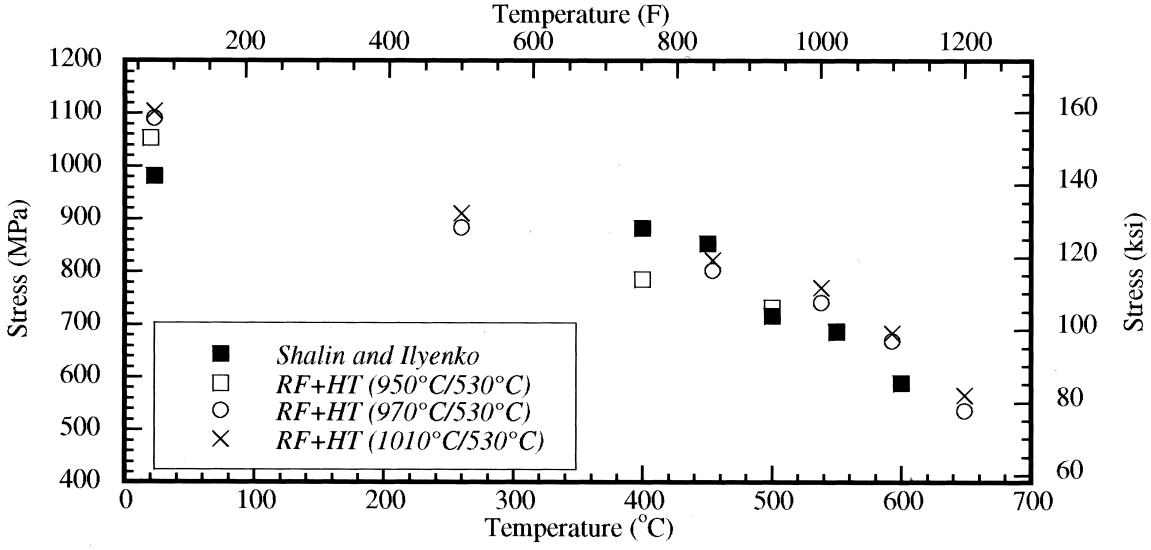

Fig. 11. The ultimate tensile strength of RF VT25 as a function of temperature.

Table 2
Stress rupture life as a function of temperature and stress for RF VT25

Temperature (°C)	Sample orientation	Heat treatment (°C)	Stress (MPa)	Rupture life (h)	Elongation (%)	Reduction in area (%)
500	Longitudinal	970	630	126.5	22	58
550	Longitudinal	970	440	87	31	59
600	Longitudinal	970	220	152	35.6	63
499	Tangential	970	621	154.5	19	58
538	Tangential	970	483	121.6	29	67
499	Tangential	1010	621	272.8	19	58
538	Tangential	1010	483	170.8	15	33

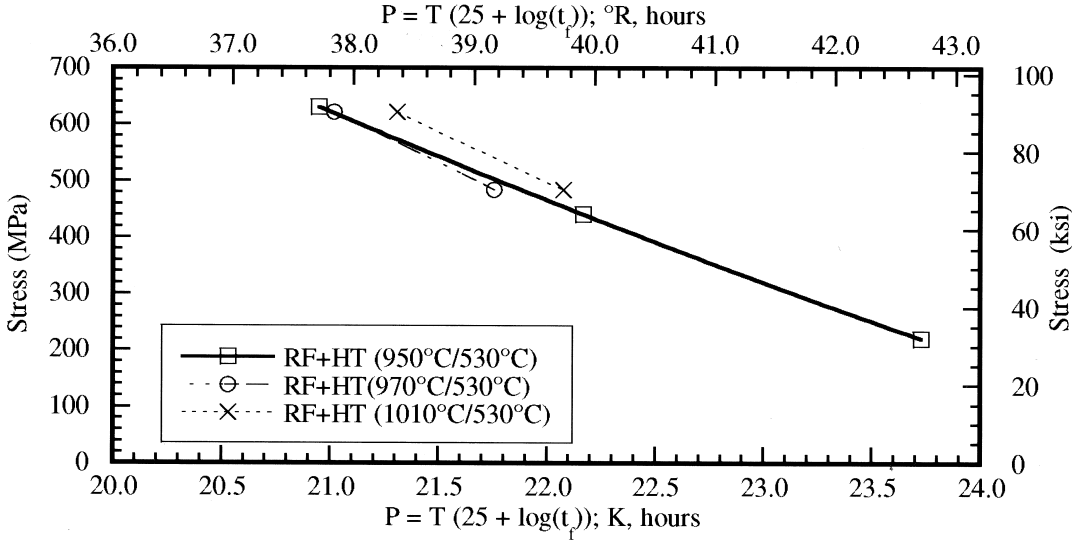

Fig. 12. Stress to failure as a function of the Larson-Miller parameter for RF VT25. Data for RF VT25 are compared with those for conventionally forged VT25.

the synthetic flaws in the RF VT25 and UFG Ti-6242 are ~20 dB higher than those of the synthetic flaws in the conventionally processed Ti-6242.

6. Mechanical property evaluation

The tensile behavior and creep properties of the RF VT25 were determined and compared with conventionally processed VT25 and Ti-6242. The yield stress and ultimate tensile stress (UTS) are shown in Table 1. The UTS of RF VT25 after three different solution treatments for test temperatures up to 650°C is shown in Fig. 11. The RF VT25 that was solution treated at 1010°C shows an increase in UTS of ~50 MPa at temperatures above 500°C over that of VT25 reported by Shalin and Ilyenko [3]. Given the maximum application temperature of VT25, the 1010°C heat treatment probably offers little tensile strength benefit over the 950°C treatment. The tensile strength of the RF VT25 that was solution treated at 950°C was also slightly higher than that of the conventionally forged VT25, which was probably a result of the smaller grain size.

Table 3
Creep data as a function of temperature and stress for RF VT25[a]

Temperature (°C)	Sample orientation	Stress (MPa)	Time to 0.2% creep (h)	Time to 0.5% creep (h)
538	Tangential	448	3.9	24.7
566	Tangential	310	11.2	34.2
607	Tangential	172	11.6	34.5
649	Tangential	138	1.5	8.9

[a] The RF VT25 was heat treated at 1010°C for 2 h and then aged at 530°C for 6 h.

The creep rupture stress is shown as a function of the Larson-Miller parameter for the RF VT25 after the three separate solution treatments in Fig. 12. The stress rupture data are also shown in Table 2. These data suggest that the 1010°C solution treatment offers a slight improvement in rupture performance over the RF VT25 solution heat treated at lower temperatures. The stress rupture life of the RF VT25 at 1000 F and 500 MPa was ~400% longer than that of $\alpha - \beta$

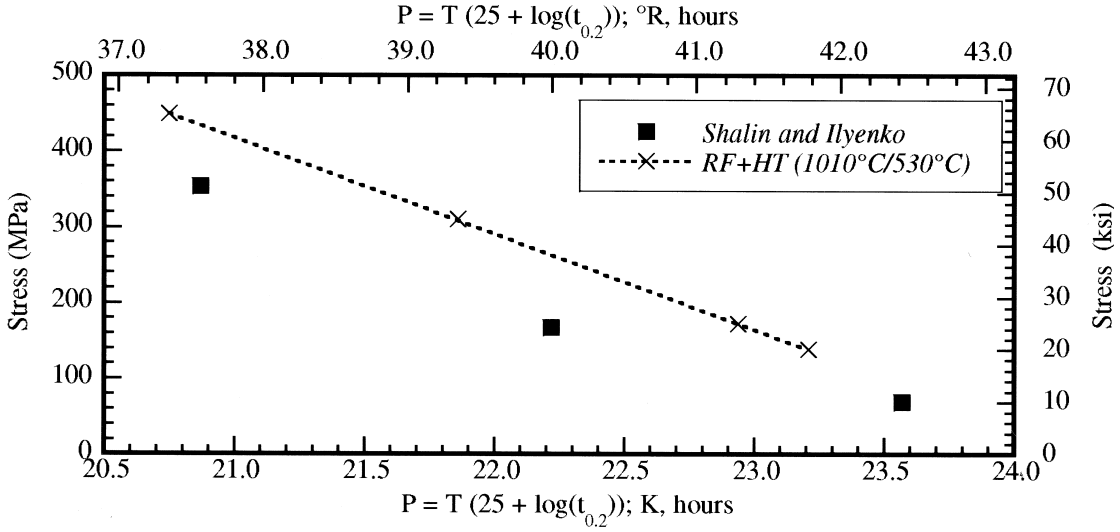

Fig. 13. Stress to 0.2% creep as a function of the Larson-Miller parameter for RF VT25.

processed Ti-6242. Furthermore, the stress rupture life of the RF VT25 at 930 F and 630 MPa was ~60% longer than Ti-6242. It has been postulated that the improved creep performance is a result of the finer scale of the transformation products of the β Ti grains [6].

Fig. 13 shows the creep stress as a function of Larson-Miller parameter of time to 0.2% creep for the RF VT25 heat treated at 1010°C and compares these data with that of Shalin and Ilyenko for conventionally processed VT25 [3]. The creep data are also shown in Table 3. These data suggest that the RF VT25 heat treated at 1010°C possesses an improvement in creep rupture performance of approximately half a Larson-Miller parameter over conventionally processed VT25 [3].

7. Summary

The present paper has described roll forming of alloy VT25. Two RF VT25 disks were evaluated and the net shape manufacturing potential of roll forming has been investigated. Both the RF VT25 disks had homogeneous macrostructures and microstructures. Electron back scattering pattern analysis indicated that the disks were essentially free of any crystallographic texture and they possessed a uniform primary α Ti grain size of ~10 μm.

The ultrasonic characteristics of the VT25 disk have been described. The RF VT25 possessed promising ultrasonic inspection characteristics and provided an increase in signal to noise for synthetic flaws of ~20 dB. The fine grain size and absence of texture were responsible for low ultrasonic noise and high inspectability. The UTS and stress rupture performance of the RF VT25 were similar to that of conventionally processed VT25. Alternative heat treatments were also used to provide some UTS and creep performance enhancements.

Acknowledgements

The authors would like to acknowledge L.C. Perocchi for the microscopy and sample preparation, S. Sitzman for the texture measurements, and Dr R.S. Gilmore for guidance with the ultrasonic measurements. The authors would also like to thank Prof. G.A. Salishev, and Drs R.M. Galeyev and O.R. Valiakhmetov for their contributions to the VT25 mechanical property evaluations. The authors would also like to thank D. Furrer, Ladish Co., for very helpful discussions.

References

[1] Furrer D. Adv Mater Processes 1999;3:33–36.
[2] The iron age 1918;102(9):491–495.
[3] Shalin RE, Ilyenko VM. Titan 1/2:23–29.
[4] Woodfield AP, Gorman MD, Corderman RR, Sutliff JA, Yamron B. In: Blenkinsop PA, Evans WJ, Flower HM, editors. Proceedings of the Eighth International Conference on Titanium, Titanium '95. London: The Institute of Materials, 1996:1116–1123.
[5] Kaibyshev OA. Superplasticity of alloys, intermetallides, and ceramics. Berlin: Springer Verlag, 1992.
[6] Lüterjing G, Levin I, Tetyukhin V, Brun M, Anoshkin N. In: Blenkinsop PA, Evans WJ, Flower HM, editors. Proceedings of the Eighth International Conference on Titanium, Titanium '95. London: The Institute of Materials, 1996:1050–1057.